Received: 24 January 2018 | Revised: 4 June 2018 | Accepted: 10 June 2018

DOI: 10.1002/mrm.27443

FULL PAPER

Magnetic Resonance in Medicine

Orientation dependence and decay characteristics of T_2* relaxation in the human meniscus studied with 7 Tesla MR microscopy and compared to histology

Benedikt Hager[1,2,3] | **Sonja M. Walzer**[4] | **Xeni Deligianni**[5,6] | **Oliver Bieri**[5,6] | **Andreas Berg**[7] | **Markus M. Schreiner**[1,2,4] | **Martin Zalaudek**[1,2] | **Reinhard Windhager**[4] | **Siegfried Trattnig**[1,2,3] | **Vladimir Juras**[1,2,8]

[1]Department of Biomedical Imaging and Image-guided Therapy, High Field MR Centre, Medical University of Vienna, Vienna, Austria

[2]CD Laboratory for Clinical Molecular MR Imaging, Vienna, Austria

[3]Austrian Cluster for Tissue Regeneration, Ludwig Boltzmann Institute for Experimental and Clinical Traumatology, Vienna, Austria

[4]Department of Orthopedics and Trauma Surgery, Medical University of Vienna, Vienna, Austria

[5]Division of Radiological Physics, Department of Radiology, University of Basel Hospital, Basel, Switzerland

[6]Department of Biomedical Engineering, University of Basel, Allschwil, Switzerland

[7]Center for Medical Physics and Biomedical Engineering, Medical University of Vienna, Vienna, Austria

[8]Department of Imaging Methods, Institute of Measurement Science, Slovak Academy of Sciences, Bratislava, Slovakia

Correspondence
Siegfried Trattnig, High Field MR Centre, Department of Biomedical Imaging and Image-guided Therapy, Medical University of Vienna, Lazarettgasse 14, A-1090 Vienna, Austria.
Email: siegfried.trattnig@meduniwien.ac.at

Funding information
Austrian Science Fund (FWF), Grant/Award Number: KLI 541-B30; Austrian Federal Ministry of Science, Research and Economy. National Foundation for Research, Technology and Development

Purpose: To evaluate: (1) the feasibility of MR microscopy T_2* mapping by performing a zonal analysis of spatially matched T_2* maps and histological images using microscopic in-plane pixel resolution; (2) the orientational dependence of T_2* relaxation of the meniscus; and (3) the T_2* decay characteristics of the meniscus by statistically evaluating the quality of mono- and biexponential model.

Methods: Ultrahigh resolution T_2* mapping was performed with ultrashort echo time using a 7 Tesla MR microscopy system. Measurement of one meniscus was performed at three orientations to the main magnetic field (0, 55, and 90°). Histological assessment was performed with picrosirius red staining and polarized light microscopy. Quality of mono- and biexponential model fitting was tested using Akaike Information Criteria and F-test.

Results: (1) The outer laminar layer, connective tissue fibers from the joint capsule, and the highly organized tendon-like structures were identified using ultra-highly resolved MRI. (2) Highly organized structures of the meniscus showed considerable changes in T_2* values with orientation. (3) No significant biexponential decay was found on a voxel-by-voxel–based evaluation. On a region-of-interest–averaged basis, significant biexponential decay was found for the tendon-like region in a fiber-to-field angle of 0°.

Conclusion: The MR microscopy approach used in this study allows the identification of meniscus substructures and to quantify T_2* with a voxel resolution

approximately 100 times higher than previously reported. T_2* decay showed a strong fiber-to-field angle dependence reflecting the anisotropic properties of the meniscal collagen fibers. No clear biexponential decay behavior was found for the meniscus substructures.

KEYWORDS
biexponential, histology, magic angle, meniscus, T2* mapping, variable echo time

1 | INTRODUCTION

Optimal meniscus function and integrity is of critical importance for the knee joint. Degeneration, tear and extrusion, and partial or full meniscectomy may lead to cartilage volume loss and put at risk for the subsequent development of premature knee osteoarthritis.[1,2] Therefore, noninvasive detection of early changes in the meniscal structure would be the prerequisite for identification of patients at risk for tear and further therapeutic decision making, to preserve meniscus tissue and delay early onset of the degenerative process of the knee joint. For cartilage, MRI increasingly caters to this need. However, the human meniscus—being of fibrocartilage tissue—is known to contain primarily short T_2/T_2* components. Hence, with conventional clinical MR sequences, the MR signal of healthy meniscal tissue decays too rapidly and appears hypointense or dark.[3,4] As a result, conventional MRI techniques, such as proton-density–, T_2– and T_1–weighted imaging can only detect tears and late-stage degenerations of the meniscus.

In recent years, advanced MRI imaging techniques, such as T_2* mapping with ultrashort echo times or variable echo times (vTE), gained increasing interest,[5-7] because they overcome limitations of conventional clinical sequences. In this context, it is of particular interest to establish correlations between quantitative T_2* measurements and biological changes in the collagen alignment as well as in the extracellular matrix (ECM), both visualized with histochemical methods.

The rationale for investigating T_2* values in highly ordered collagen fiber tissue relates to the relationship between T_2* and the condition of the ECM; that is, the complex array of collagen, glycoproteins, and proteoglycans. Additionally, myxoid changes, fibrocartilaginous separation of the matrix, extensive fraying, and tears[8] are accompanied by a loosening of collagen fiber organization and increasing water content[9] and are found to increase T_2* values.[6,7]

Recent studies have suggested that T_2* decay in the meniscal tissue can be described by a biexponential function, where the short and long component of T_2* are suggested to reflect bound and free (bulk) water pools.[7,10] Moreover, it was found that the short component of T_2* might contain additional information about the collagen matrix, and that it provides greater ability for distinguishing between normal and degenerated meniscus.[7] Accordingly, high-resolution mono- and biexponential quantitative T_2* mapping is a method with great potential for noninvasive detection of structural and degenerative changes in meniscal tissue.[6,7] However, to date, the mechanisms of mono- and biexponential decay in human meniscus are still not fully understood.

The orientational collagen fiber to magnetic field angle dependence as a result of residual dipolar coupling is a well-known property of highly ordered collagen structures, such as tendon,[11-14] cartilage,[15] and meniscus.[16] Dipolar interaction of protons in the collagen network is modulated by the term[17] (Equation (1)):

$$D \sim 3cos^2\theta - 1, \quad (1)$$

where θ is the collagen fiber to magnetic field angle (or short, fiber-to-field angle). At $\theta = 55°,125°$, etc., the so-called magic angles, all water protons tend to resonate at the same frequency, which results in an increase of effective T_2/T_2* values.[17] Orientation dependence of meniscus T_2* values has not yet been evaluated.

The aims of this study were to: (1) show the feasibility of in vitro mono- and biexponential T_2* analysis of degenerated human meniscus specimens using a 3D vTE sequence with microscopic pixel resolution and compare T_2* results to histological findings; (2) use quantitative MR microscopy to investigate how T_2* values within different meniscal zones vary depending on the circumferential fibers (the predominant fiber type making up the bulk of the meniscus, as previously described[18,19]) to the main magnetic field; and (3) increase understanding of T_2* decay characteristics and water compartmentalization in human meniscus by statistically evaluating the preference of a mono- versus a biexponential model on a voxel-by-voxel– as well as on a region-of-interest (ROI)–averaged basis.

2 | METHODS

2.1 | Sample preparation and MR methods

Meniscus specimens were obtained with written informed consent from two osteoarthritis (OA) patients with no

documented meniscal lesions undergoing knee replacement surgery in accord with the terms of the ethics committee of the Medical University of Vienna (EK-Nr: 1065/2011), following the guidelines of the Declaration of Helsinki and Tokyo.

All MRI experiments were performed on an ultra-high-field 7 Tesla (T) whole-body system (Magnetom Siemens Healthineers, Erlangen, Germany), using a microimaging system[21] providing a maximum gradient strength of 750 mT/m.

2.2 | Experiment 1: correlation of T_2* maps with histological assessment

In total, five meniscal segments were obtained from a pair of human lateral and medial menisci from the same OA knee joint (age: 60 years, female; Kellgren-Lawrence Score: 4; Knee Society Score: 58/60), from which three representative segments were obtained from the medial meniscus (body, posterior horn, and anterior horn, further denoted as segments 1, 2, and 3, respectively) and two representative segments were obtained from body and the posterior horn of the lateral meniscus fragment (further denoted as segments 4 and 5, respectively).

For T_2* mapping a 19-mm ^{1}H-NMR volume coil (Rapid Biomedical, Wuerzburg, Germany) was used. For quantitative monoexponential T_2* assessment, a 3D vTE sequence was used.[22] The sequence is based on a gradient echo spoiled sequence, but was modified to use a highly asymmetric readout and a variable echo time approach in phase and slice encoding direction to dynamically adapt and shorten the echo time toward the center of k-space. A short (150-μs) nonselective hard radiofrequency (RF) pulse was applied for excitation and RF (phase cycling) and gradient spoiling were used to disrupt residual transverse magnetization and minimize repetition time. This concept allows fast high-resolution measurements with effective echo times in the submillisecond range. In addition, the sequence uses projection onto convex sets formalism for reconstruction of the undersampled data set.[22,23]

In this experiment, data for T_2* maps were acquired using a series of single-echo vTE scans. This was done to ensure that the T_2* decay of the meniscus, especially the short echo range (around 0.5-2.5 ms), was adequately covered by all echoes. Moreover, given the short T_2* values of meniscus, these short echo times are critical to gain high signal-to-noise ratio (SNR).

To resolve the structures of the meniscus, the resolution along the triangular cross-section of the meniscus was given priority. To this end, microscopic in-plane pixel resolution (<100 μm) with high SNR, that is needed for T_2* mapping, was achieved at the expense of lower slice resolution (slice thickness = 400 μm) along the circumferential collagen fiber direction (i.e., the third dimension of the voxel).

The following echo times (TEs) were used: 0.4, 0.7, 1.2, 1.7, 2.5, 4, 6, 8, and 12 ms. Other imaging parameters were: field of view (FOV) = 12×14 mm^2, pixel size = 60×60 μm^2, slice thickness = 0.4 mm, number of slices = 22, repetition time (TR) = 25 ms, flip angle (FA)[24] = 9°, signal averages = 4, and acquisition duration = 90 minutes.

2.3 | Experiment 2: fiber-to-field angle dependence

Anisotropic analysis was performed on one human lateral meniscus fragment (age: 64 years, female; Kellgren-Lawrence Score: 4; Knee Society Score: 42/50, posterior horn was removed during surgery), using the same 7 T microimaging setup. In contrast to the previous measurement, a 39-mm ^{1}H-NMR volume coil (Rapid Biomedical) was used. In order to image the meniscus specimen in different orientations, it was fastened on a plastic cross using thread and then imbedded in the middle of a 30-mm-diameter plastic sphere filled with physiological saline solution. For morphological evaluation of the meniscus structure, a proton-density-weighted spin-echo sequence was used. Imaging parameters were: TE = 6.4 ms, TR = 3500 ms, FA = 180°, FOV = 30×30 mm^2, matrix = 448×448, pixel size = 67×67 μm^2, slice thickness = 0.4 mm, slice offset = 100%, and number of slices = 14.

Mono- and biexponential T_2* assessment was performed on data acquired with the 3D vTE sequence. In this experiment, a multi-echo approach was applied. Image parameters included: 12 TEs = 0.82, 1.82, 2.82, 7.23, 9.23, 11.23, 13.39, 15.39, 17.39, 19.55, 21.55, and 23.55 ms, TR = 38 ms, FA = 17°, FOV = 30×30 mm^2, matrix = 448×448, pixel size = 67×67 μm^2, slice thickness = 0.4 mm, number of slices = 72, signal averages = 1, and acquisition duration = 48 minutes. Water selective binomial 1-1 excitation (a pair of 150-μs pulses) was used to null possible signal from the fat.[25,26] All measurements (PD-weighted, T_2* mapping) were performed in both axial and coronal direction of the meniscus. The sample was positioned in a way to be reasonably sure that the orientation of most of the circumferential fibers with respect to the main magnetic field was: 0°, 55°, and 90°.

These angles were chosen for the following reasons: At 0°, the dipolar interaction is at a maximum and all water protons related to collagen fibers tend to resonate at different frequencies, which results in expected lowest effective T_2 and T_2* values. In contrast, at the magic angle (55°), all water protons tend to resonate at the same frequency, which results in the expected highest effective T_2/T_2* values.[17] The 90° angle was chosen because it reflects a similar angle to the in vivo case of the meniscus in a horizontal MR scanner.

In this regard, the plastic sphere and the cross, where the meniscus fragment is fastened on, were used for positioning and alignment of the FOV and thus the slices, ensuring equally aligned slices for each orientation.

ROIs were defined in 3 different areas (tendon-like tissue, fibrous tissue from the external circumference, and fibrous tissue from the internal circumference) representing the variability in human meniscus. Subsequent ROI analysis (voxel-wise– and on an ROI–averaged basis) was performed on 10 consecutive slices from the meniscus body in 3 orientations and for all sets of ROIs.

2.4 | Image postprocessing

Calculation of mono- and biexponential T_2* analysis was performed using a nonlinear Levenberg-Marquardt (LM) algorithm curve-fitting method,[27,28] which was conducted using a custom-built IDL script (Interactive Data Language; Research Systems, Inc, Boulder, CO), using the mpcurvefit library,[29] and was done on a voxel-by-voxel basis with a confidence interval of 95%.

For monoexponential fitting, a 3-parameter model fitting was used (Equation (2)):

$$S_m = A_1 e^{\frac{-TE}{T_2^*}} + \varepsilon, \tag{2}$$

where A_1 is the maximum signal at t = 0, which is also often described as a product of proton density (S_0) and a proportionality constant (k) subsuming signal gain or attenuation by the scanner's hard-/software ($A_1 = k\ S_0$). T_2* corresponds to the actual monoexponentially calculated T_2* value, and ε is the offset. The offset can be seen as a non-zero baseline that takes into account the signal that has not converged toward zero.[30]

The initial parameter value for the monoexponential T_2* component was given as T_2* = 10 ms, which should be a good estimation according to literature.[7] It should be noted, however, that the LM fit is reasonably insensitive to the starting values of the parameters.[31] Therefore, if initial values are slightly off, usually the fit still leads to good results, which is an important property for this evaluation, because the meniscus is a very heterogeneous structure with different T_2* values.

The same MRI data were also fitted by a biexponential decay curve, using a 5-parameter model function (Equation (3)):

$$S_m = B_1 e^{\frac{-TE}{T_{2s}^*}} + B_2 e^{\frac{-TE}{T_{2l}^*}} + \varepsilon \tag{3}$$

where T_2*$_s$ refers to the short T_2* component and T_2*$_I$ to the long component of T_2*. B_1 and B_2 are the component ratios. ε is the baseline offset given primarily by noise.

Initial parameter values for the biexponential T_2* components were set to T_2*$_s$ = 2 ms for the short T_2* component and T_2*$_I$ = 15 ms for the long component based on a priori information from the literature.[7,10] Moreover, lower and upper boundary constraints of the parameters were chosen, where for short components the limits are: [0, 20 ms], and for the long components: [0, 200 ms].

In order to test whether individual meniscus voxels show mono- or biexponential T_2* decay, we compared the quality of mono- and biexponential model fitting using Akaike information criteria (AIC).[32]

In general, adding supplementary parameters allows to increase the likelihood of a model, but this introduces the possibility of overfitting.[33] In other words, the model with fewer parameters will almost always fit the data worse. Consequently, AIC adds a penalty term for the number of parameters. In our specific case, the number of data points (n = 12) is rather low compared to the number of parameters (k = 3 and 5, for mono- and biexponential model, respectively); therefore, a small-sample (second order bias corrected) Akaike information criterion (AIC_C) was used.[34] Assuming that the scatter of data points around the best fitted curve follows a Gaussian or normal distribution with constant variance (which is usually assumed in nonlinear regression), then the AIC_C can be given as follows (Equation (4)):

$$AIC_C = 2k + n\log\left(\frac{SSE}{n}\right) + \frac{2k(k+1)}{n-k-1}, \tag{4}$$

where n refers to the number of data points, k is the number of parameters, and SSE is the standard error of the estimate. The model with the lower AIC_C is more likely the one being correct.

Additionally, we also used F-tests to compare the goodness of fit of the mono- and biexponential model and assess, for each voxel, whether a biexponential model is more appropriate over a monoexponential model. This was evaluated by comparing the standard error of the estimate adjusted for the number of degrees of freedom[35] (Equation (5)):

$$F = \frac{\left(SSE_{mono} - SSE_{bi}\right)}{SSE_{bi}} \frac{v_{bi}}{v_{mono} - v_{bi}} \tag{5}$$

where SSE_{mono} and SSE_{bi} are the standard error of the estimate (SSE) of the mono- and biexponential fits, respectively, and v_{mono} and v_{bi} are the degrees of freedom of both analyses (v = n – k). The *P* value of the associated F-ratio was then calculated based on F-distribution. All statistical analyses were performed setting the critical significance level to 5%. For a *P* value smaller than an α-level of 0.05, the biexponential model was considered preferable. Vice versa, the monoexponential model was considered preferable. In contrast to AIC_C, F-test is a null-hypothesis test that has the prerequisite that the models must be nested, which is the case for the mono- and biexponential models.

For each slice, F-test and AIC_C were performed between a mono- and a biexponential model, and from the results the

following maps are calculated: $T_2{}^*_s$ map of the biexponential T_2* analysis for the short relaxing component, $T_2{}^*_I$ map of biexponential T_2* analysis for the long component, a binary map depicting voxels that can be preferentially considered biexponential (0 = monoexponential decay, 1 = biexponential decay), and short and long T_2* component fraction maps. Additionally, a monoexponential T_2* map ($T_2{}^*_m$) was calculated for each slice.

Moreover, F-test and AIC_C were used to test whether individual selected regions of interest showed mono- or biexponential T_2* decay type on an ROI–averaged basis.

2.5 | Statistical analysis

Grand mean T_2* ($T_2{}^*_m$) values of all of the slices of the meniscus segments were calculated using the weighted mean values (weighted by number of voxels per slice) of the mean T_2* of each slice.

From the ROIs of the 10 slices of the orientational analysis, mono- and biexponential T_2* analyses were performed. Bartlett's test[36] was used to test for heteroscedasticity. For a P value > 0.05, the variances are homogeneous and the data set is considered homoscedastic. Depending on the result of Bartlett's test, three-way analysis of variance (ANOVA) and Welch's ANOVA were then performed to test for statistical significance. A P value ≤ 0.05 was considered to indicate statistically significant results. All statistical analysis was performed using R Statistical Software (version 3.2.3[37]; R Foundation for Statistical Computing, Vienna, Austria). Box plots were created using the *ggplot2* package[38] and an extension, *ggsignif*.[39]

2.6 | Histological assessment

Following the MR measurement, the triangle-shaped meniscus cross-sections were fixed with neutral-buffered 4% formaldehyde and embedded in paraffin after decalcification. After deparaffination through xylene and graded alcohol, 2.5-µm serial slices were stained with hematoxylin-eosin, used for the morphological overview. Picrosirius red (PSR) staining was used for detection of collagen under light microscopy and visualizing collagen alignment by polarized light microscopy (PLM; Zeiss, Oberkochen, Germany). Under polarized light, birefringence of collagen fibers allows to define the collagen architecture of tissue. The combination of PSR and Alcian blue staining provides further information about local changes of increasing cartilaginous differentiation in the ECM during the process of degeneration.

3 | RESULTS

Figure 1 shows a representative microscopic T_2* map (Figure 1A) of one segment of the body of a medial meniscus (segment 1) and the corresponding PSR-stained slice using a polarized light filter (Figure 1B). The first (TE = 0.4 ms) and the eighth echo image (TE = 8 ms) of the single-echo sequence are shown in Figure 1C and 1D, respectively. This meniscus segment was measured with the circumferential fibers oriented at approximately 0° to the main magnetic field (B_0). Noteworthy, there is a striking similarity between the T_2* map, the eighth echo image, and the histological assessment of PSR staining under polarized light.

The first echo time image measured with TE = 0.4 ms (Figure 1C) shows high SNR (~35) for all of the meniscal microstructures, whereas, for instance, for an echo time of TE = 8 ms (Figure 1D), many parts of the meniscus (particularly highly ordered circumferential fibers) display little to no signal and provide a hypointense background for the fibrous network, which is well depicted with this echo time.

Qualitatively, the results show that thick fibrous bundles penetrate through the meniscus cross-section from the outer vascularized zone into the inner avascular zone. As mentioned earlier, this meniscus sample was measured with the circumferential fibers parallel to the main magnetic field. With this fiber-to-field orientation and setup, the overall mean T_2* value of segment 1 is 7.9 ± 4.5 ms.

In this sample, circumferential fiber bundles show relatively short T_2* values as depicted by an ROI assessment (ROI1, white rectangle in Figure 1A), which shows a mean T_2* value of 4.4 ± 0.9 ms. This region in the external circumference is further denoted as a tendon-like region, because it histologically resembles to tendon tissue.[19]

For the fibrous bundles, T_2* values are much higher as exemplarily depicted by ROI2 (black rectangle) in Figure 1A, which shows a mean T_2* value of 15.5 ± 3.9 ms. Other fibrous regions are depicted by yellow arrows (Figure 1A,B).

Moreover, the laminar outer layer, which has a thickness of around 200 µm,[19] can clearly be visualized by this measurement setup as depicted by close-up images of the T_2* map and the PSR-stained image measured with polarized light (Figure 1E and F, respectively). The position of the close-up images is demarked by white asterisks in Figure 1A and B.

The T_2* values of the laminar outer layer are higher compared to circumferential fibers as exemplarily depicted by an ROI (black rectangle) in the close-up image of the T_2* map (Figure 1E), which shows a mean T_2* value of 11.7 ± 2.1 ms.

For all meniscus samples and slices from experiment 1, the percentage of voxels that can preferentially be considered biexponential is extremely low (<3%), when tested with AIC_C and F-test. The results of experiment 1 are summarized in Table 1.

Figure 2 depicts one meniscus specimen measured in three different orientations to the magnetic field. The schematic drawings of Figure 2 (A1, A2, and A3) show how the meniscus sample was measured with respect to

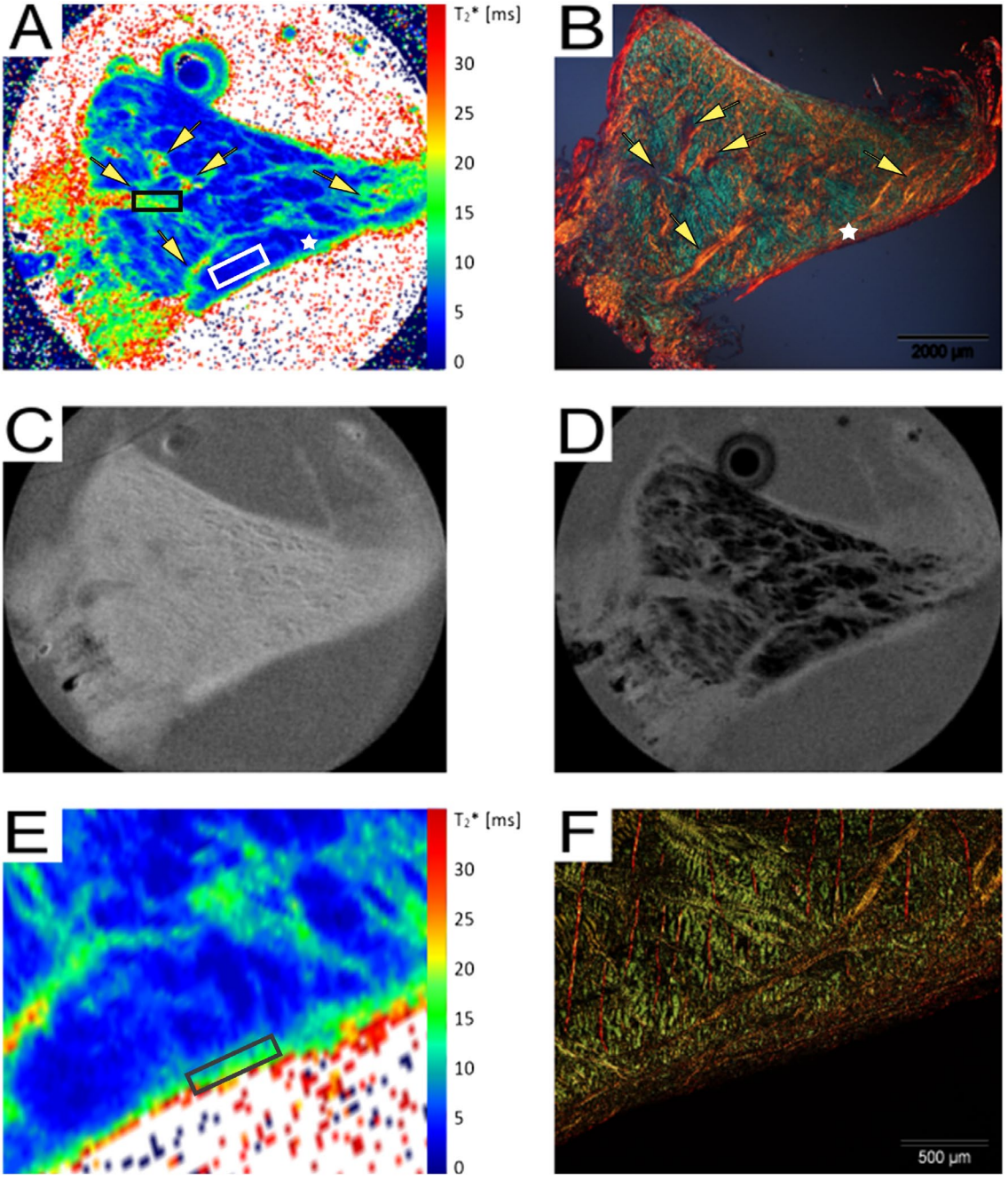

FIGURE 1 A, T_2* map of the body of a degenerated medial human meniscus measured with a 3D vTE sequence. ROIs are depicted in the region of highly ordered circumferential fibers (ROI1, white) and fibrous tissue from the external circumference (ROI2, black). Yellow arrows show fibrous tissue. The white asterisk depicts the area that is shown as a close-up in (E). B, Shows the corresponding PSR-stained slice measured using polarized light filter with 10 × magnification. Again, yellow arrows show fibrous tissue and the white asterisk depicts the area that is shown as a close up in (F). C, The first echo image (TE = 0.4 ms) shows high signal intensity for all meniscal substructures. D, The eighth echo image (TE = 8 ms) depicts the fibrous network of the meniscus. The signal from the highly ordered circumferential fibers is almost completely gone with this echo time. E, Close-up image of the T_2* map depicts the lamellar-like layer of the meniscus. F, Close-up image of the PSR-stained slice measured using polarized light (40 × magnification) indicates the outer lamellar-like layer of the meniscus

the main magnetic field: 0° (Figure 2A1), 55° (Figure 2A2), and 90° (Figure 2A3). Figure 2 (B1, B2, and B3) shows T_2* maps from the same representative zone from the body of the meniscus measured in the respective fiber-to-field angles.

The magic angle orientation (55°) showed highest T_2* values with a grand mean value of 27.1 ± 1.0 ms, whereas at a fiber-to-field angle of 0° the T_2* values were lowest (T_2* = 18.8 ± 1.3 ms). At 90°, T_2* values were found to be in between, with mean values of T_2* = 24.2 ± 1.8 ms.

TABLE 1 Summary of mean T_2* (T_2*$_m$) values and of percentages of voxels that can preferentially be considered to show biexponential decay

Segment nr. (voxel-wise)	T_2*$_m$ [ms]	AIC_C [%]	F-test [%]
SEG. 1	7.9 ± 4.5	<1%	<1%
SEG. 2	11.4 ± 7.7	2%	2%
SEG. 3	8.5 ± 5.3	<1%	<1%
SEG. 4	12.9 ± 4.9	<1%	<1%
SEG. 5	11.5 ± 6.3	<1%	<1%

There was zonal variation in T_2* values, which was highly dependent on the orientation of the collagen fibers to the magnetic field. This is depicted by ROIs in a representative proton-density-weighted image of the meniscus body (Figure 3B). The results of the voxel-by-voxel evaluation are presented in box plots (Figure 3 (C1–C3)).

Tendon-like structure located in the external circumference (depicted as blue ROI in Figure 3B) showed the strongest orientational dependence, reflecting the highly anisotropic collagen fiber architecture of these structures and the consequential incomplete averaging of dipolar coupling (Figure 2 (B1-B3), 3 C1). At the magic angle, the mean T_2* value of this region was 12.19 ± 1.56 ms, whereas at 0° the mean value was 3.3 ± 0.5 ms, which equals an approximate 400% difference between values at these orientations. In contrast, fibrous-like tissue from the external circumference and fibrous-like tissue from the internal circumference showed less angle-dependent changes (Figure 2 (B1-B3), 3 (C2-C3)).

Voxel-wise analysis, using AIC_C and F-tests, revealed that biexponential pixels can only be found in the tendon-like region of the meniscus. Exemplarily, Figure 4A shows one representative binary map depicting pixels that can be considered biexponential according to AICc. Figure 4B shows the corresponding morphological echo image with a TE of 13.39 ms.

For ROI-averaged analysis, the SNR is increased by approximately a factor of 10 to 100, because SNR adds by $\sqrt{n}$,[40] where n is number of voxels. The results of the ROI-averaged analysis of experiment 2 are summarized in Table 2. At a fiber-to-field orientation of 0°, the tendon-like region and the fibrous tissue from the external circumference (ROI2) showed preferential biexponential decay as statistically evaluated by AIC_C and F-test. In contrast, the fibrous tissue region (ROI3) showed barely any biexponential decay in any orientation (≤10%).

For large ROIs of the white zone and red zone, as exemplarily shown in Figure 4, the T_2* decay showed biexponential decay for all 10 consecutive slices as evaluated by AIC_C and F-test.

4 | DISCUSSION

Mono- and biexponential T_2* mapping was performed on five human meniscus samples using ultrashort echo time and microscopic in-plane pixel resolution. To this end, for the first time, the relationship between T_2* values and collagen alignment of one human meniscus sample was studied based on a T_2* analysis at a series of circumferential fiber to magnetic field orientations. All MR findings were compared to histological findings.

Our study showed a zonal analysis of spatially matched T_2* maps and histology images of the human meniscus with a resolution that, to our knowledge, has not been reported yet. Moreover, our study shows a strong orientational anisotropy of T_2* values; especially for the highly ordered tendon-like region of the meniscus. Furthermore, T_2* decay showed no clear biexponential decay pattern, in contrast to the findings of previous studies (e.g., Diaz et al.[10]).

This study shows that ultrahigh field strength (7 T), in combination with a small-sample MR microimaging system, allows to visualize the human meniscus and its ultrastructure with microscopic in-plane pixel resolution and high SNR in relatively short scan time (i.e., 10 minutes for one single-echo measurement). This is both attributed to the high field strength (B_0), offering an SNR increase proportional to $B_0^{7/4}$ in theory[41] in combination with small-volume coils (19 and 39 mm), where SNR is approximately inversely proportional to the coil diameter (SNR ~ 1/d). As a result, voxel sizes of 60 × 60 × 400 μm^3 (experiment 1) and 67 × 67 × 400 μm^3 (experiment 2) became feasible, yielding a microscopic pixel resolution along two spatial directions. Overall, this yields an increase in the sensitivity by one to two orders of magnitude, as compared to conventional whole-body MRI with large coils.

Nevertheless, up until now, MR microscopy of short T_2/T_2* musculoskeletal tissue such as the meniscus is still rarely performed because of lack of hardware availability close to clinical applications (scanner, microimaging system, and coils) and sequence limitations. However, it is well known that these very-high-resolution measurements of highly organized collagen tissues are important in the field of MRI, because the results can help explain different intrinsic MR properties (T_2, T_2*, and $T_{1\rho}$) and appearances of tissue in MRI (e.g., with change in fiber-to-field orientation).

Bae et al.[42] previously showed high nominal spatial resolution (voxel size = 130 × 130 × 130 μm^3) human meniscus images using a 2D and 3D ultrashort echo time (UTE) pulse sequence. They found that using UTE sequences and shortest, sub-ms TE allows to detect high signal from all the meniscus substructures and that the fibrillar network is better depicted at TE ~ 5 ms, which is in accord with the findings presented in our study.

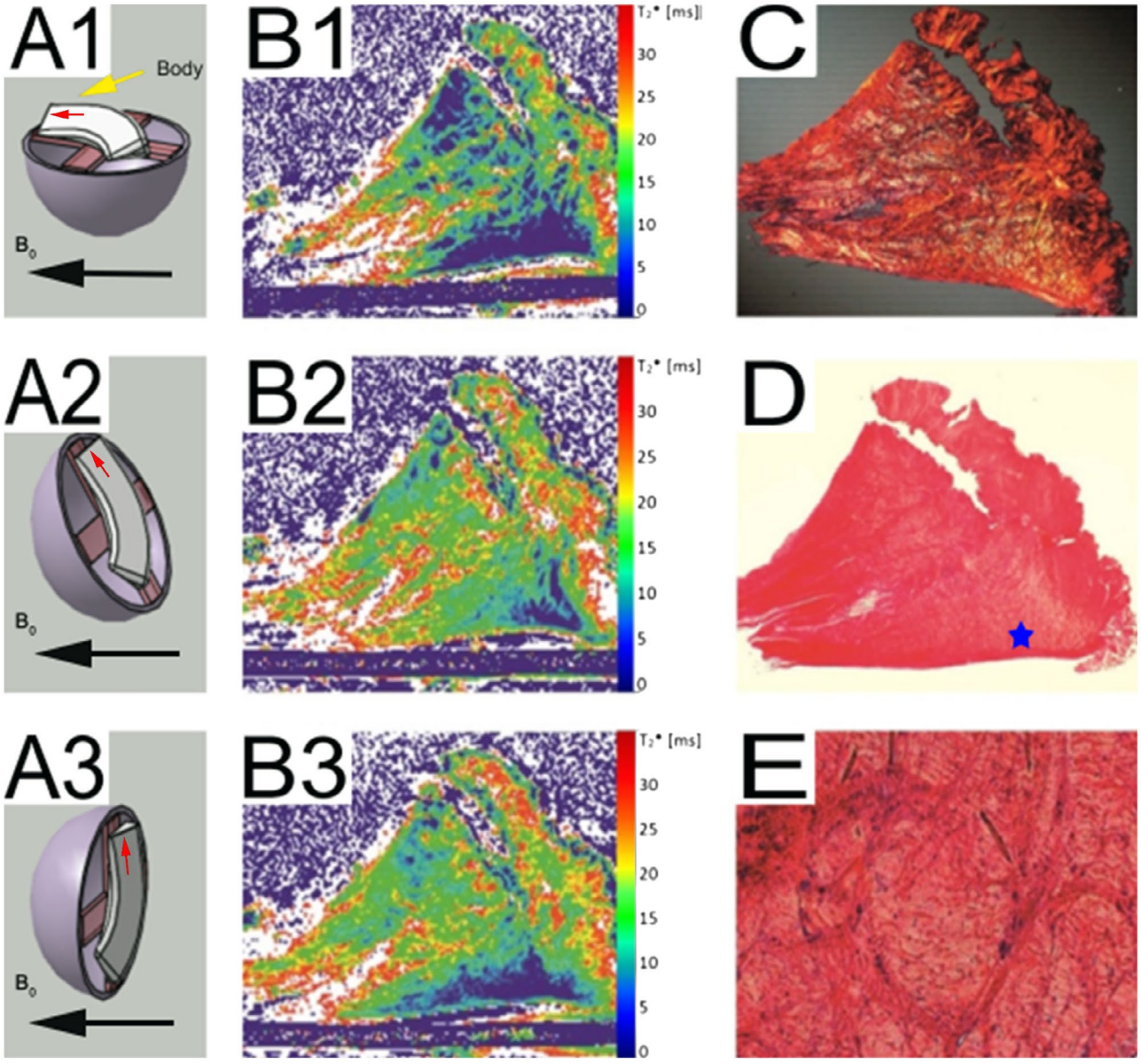

FIGURE 2 A1–A3, Schematic drawings of the fiber-to-field orientations: 0°, 55°, and 90° (A1, A2, and A3, respectively). The yellow arrow shows the position of the meniscus body, and the red arrows indicate the orientation of the circumferential fibers in this area. B1–B3, T_2* maps of 1 representative zone from the body of the meniscus with fiber-to-field angle 0° (B1), 55° (B2), and 90° (B3). C, The corresponding PSR-stained slice with polarized light visualizing the collagen fiber distribution. D, PSR/alzian blue combination stain was used for the visualization of collagen fibers and local increased appearance of glycosaminoglycans in fibrocartilaginous tissue. E, Shows a close-up of the tendon-like zone of the meniscus. The blue asterisk in D, depicts the area that is shown as a close-up

In our study, a 3D variable echo time (3D vTE) sequence was used to acquire images with ultra short echo time, which allowed to gain signal from highly ordered collagen tissue such as the meniscus. Moreover, this sequence uses a rectilinear k-space sampling scheme, where it differs from UTE sequences, which mostly use center-out radial trajectories. Consequently, the 3D vTE sequence is less prone to artefacts from k-space trajectory errors.[22] Moreover, it allows faster measurement compared to radial acquisition, which have an inherently less-efficient acquisition scheme.[43]

The sequence also benefits considerably from the strong gradients (750 mT/m) of the 7 T microimaging system and allows even shorter echo time (~0.4 ms) compared to 7 T in vivo whole-body imaging, where the minimum effective echo time is around 0.8 ms.[7]

T_2* maps and PLM images of human meniscus samples show noticeable similarities, indicating that T_2* maps are very sensitive to the heterogeneous ultrastructure in terms of collagen fiber density and their orientation. With an in-plane pixel resolution of 60×60 μm^2, we were able to visualize

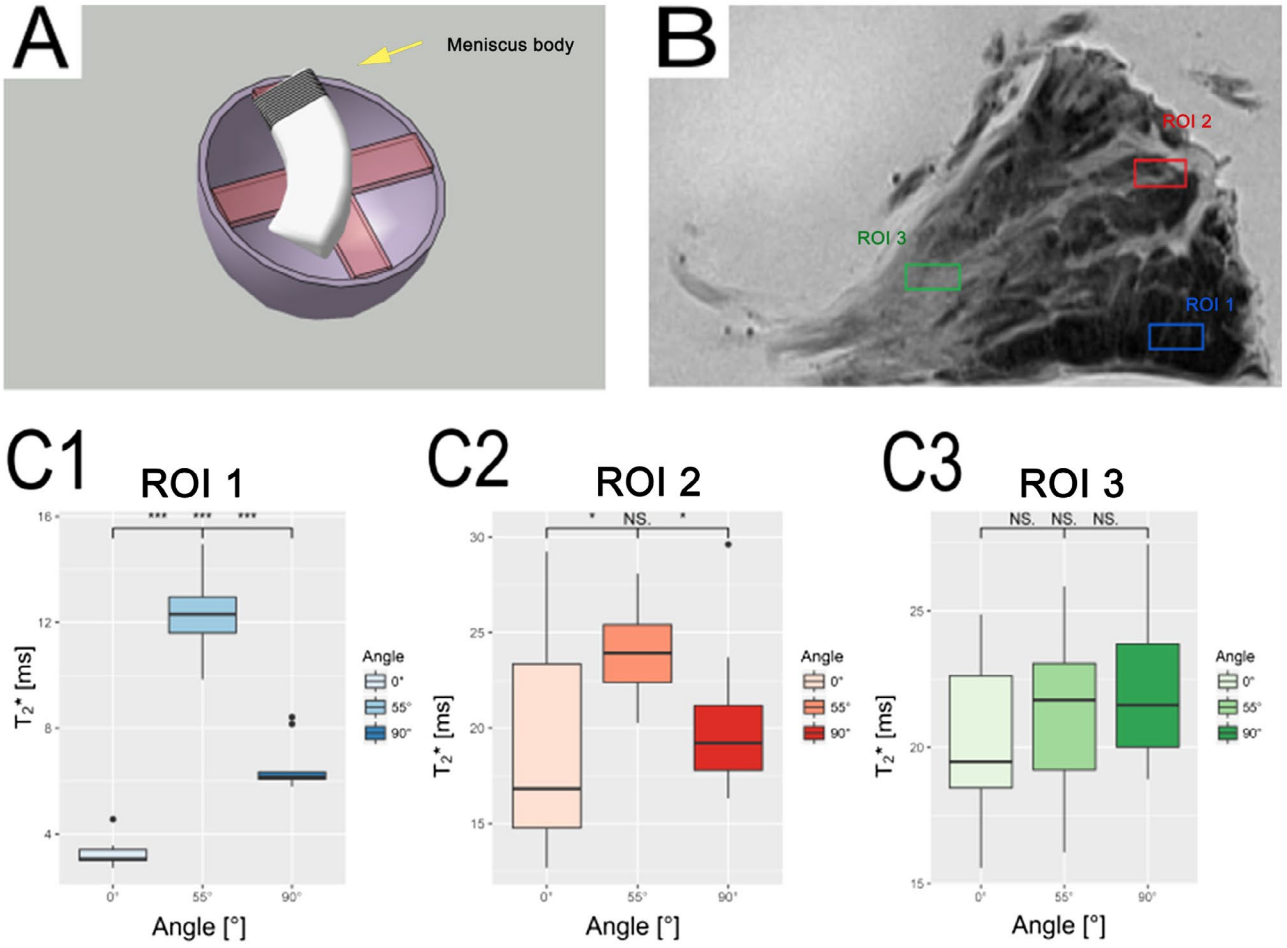

FIGURE 3 A, Schematic drawing of the position of the 10 representative coronal slices in the body of the meniscus. The meniscus sample was not complete, meaning that the posterior horn was removed during the surgery. B, Representative PD-weighted image depicting the investigated regions. ROI1 (blue) represents tendon-like structure, ROI2 (red) represents fibrous-like tissue from the external circumference, and ROI3 (green) marks fibrous-like tissue from the internal circumference. C1–C3, Box whisker plots: 10 consecutive slices from the base of the meniscus were analyzed. ROI1: tendon-like structure; ROI2: fibrous structure from the external circumference; ROI3: fibrous structure from the inner zone. The bold line near the middle of the boxes indicates the median. The bottom of the boxes indicates the 25th percentiles, whereas the top of the boxes delineates the 75th percentiles. The whiskers comprise the data up to the 1.5 interquartile range (IQR). The dots represent outliers. The asterisks in the box plots denote the level of significance (P value) between the groups: not significant (NS) = ($P > 0.05$); $^{*}(P \leq 0.05)$; $^{**}(P \leq 0.01)$; $^{***}(P \leq 0.001)$

and quantify (in terms of T_2* values): fibrous bundles, circumferential fibers, and the laminar layer.

Up until now, T_2* mapping of the meniscus using microscopic resolution, in combination with ultrashort echo time and comparison to histology, has not been performed yet. However, a comparison between T_2* values of comparatively lower resolution data (voxel size = 270 × 270 × 2000 μm^3) and a histological score was performed by Williams et al.[6] In accord with their study, we found that regions of advanced degeneration in the meniscus, such as fibrous remodeling and extensive fraying, clearly show higher T_2* values.

Furthermore, Williams et al. claimed that UTE is, strictly speaking, not required to study meniscus T_2* relaxation. Nevertheless, it was noted that the use of sub-ms echo times improves both capture and curve fitting of the short T_2* component (i.e., <6 ms) and therefore providing increased sensitivity to subtle differences between meniscus regions that may help to detect earlier changes to meniscus health.

In our study, we found that thick fibrous bundles from the joint capsule and zones of extensive fraying show higher T_2* values. Evidently, for these structures UTE is not necessary. However, for highly ordered circumferential fibers, which tend to have short T_2* values around 5 ms (depending on the fiber-to-field angle), UTE likely leads to more reliable results when studying T_2* relaxation, because considerable signal decay already occurs within the first millisecond.

In experiments 1 and 2, the number of pixels that can be considered to feature biexponential decay was extremely low as evaluated with AIC_C and F-test. This seems to be in

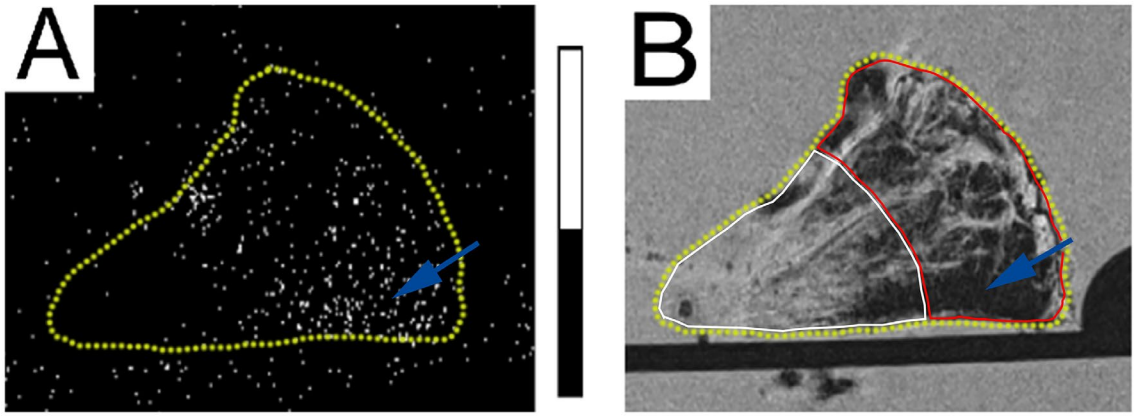

FIGURE 4 A, Shows a binary map of the pixels with biexponential (white) and monoexponential (black) signal decay when tested with AIC_C at a fiber-to-field angle of 0°. B, Shows a morphological image with TE of 13.39 ms. Biexponential pixels are primarily found in the tendon-like region (blue arrows) of the meniscus. The yellow dotted line in both images delimits the meniscus surface from the surrounding water. In case a large ROI-based analysis is performed (here depicted in B as red and white ROI for red zone and white zone of the meniscus, respectively) similar to what is used in in vivo studies, then the T_2* decay is preferentially biexponential for all 10 consecutive slices as evaluated by AIC_C and F-test

TABLE 2 Summary of results of the orientational ROI averaged analysis of experiment 2

Region	Angle [°]	T_2*$_m$ [ms]	T_2*$_s$ [ms]	T_2*$_l$ [ms]	F_s [%]	AIC_C [%]	F-test [%]
ROI1	0°	2.08 ± 0.44	1.34 ± 0.49	4.50 ± 1.98	56.14	80	80
	55°	9.98 ± 1.92	1.43 ± 0.83	11.80 ± 2.73	14.28	50	40
	90°	7.15 ± 0.35	6.59 ± 0.60	29.92 ± 13.88	84.12	0	0
ROI2	0°	9.16 ± 1.31	1.31 ± 0.80	10.69 ± 1.30	21.69	60	60
	55°	18.19 ± 2.11	0.41 ± 0.53	19.45 ± 2.19	21.30	10	0
	90°	15.40 ± 1.65	7.08 ± 6.33	18.85 ± 5.80	23.55	0	0
ROI3	0°	20.23 ± 4.48	6.02 ± 7.62	22.14 ± 5.40	18.11	10	10
	55°	19.09 ± 5.05	6.95 ± 9.13	20.29 ± 2.92	12.72	0	0
	90°	22.83 ± 7.83	11.31 ± 6.72	24.73 ± 4.14	11.15	0	0

ROI1 refers to tendon-like structure, ROI2 represents fibrous-like tissue from the external circumference, and ROI3 marks fibrous-like tissue from the internal circumference. Mean monoexponential T_2* values (T_2*m) as well as short and long component values of the biexponential analysis, T_2*$_s$ and T_2*$_l$, respectively, from 10 consecutive slices are provided. The short T_2 fraction is given as F_s. The percentage of ROIs from these 10 consecutive slices showing preferential biexponential decay behavior (according to AIC_C and F-test) is given for each of the 3 ROIs and orientations.

contradiction to the results of high-resolution T_2* mapping in vivo.[7] However, we assume that this can possibly be attributed to the compartmentalization of the meniscus. With increasing voxel size, the probability of voxels covering multiple tissue types of the meniscus (e.g., tendon-like collagen fibers and fibrous tissue together) will be increased.

However, it should also be noted that in earlier biexponential/bicomponent studies (e.g., Diaz et al.[10] and Juras et al.[7]) no model testing between mono- and biexponential model was performed. Therefore, it cannot be ruled out, that their biexponential interpretations suffer from misinterpretation attributable to overfitting.

The number of echo times used in experiment 1 (9 TEs) was similar to what was used in previous bicomponent studies[7,44]; however, this number can still be considered low for biexponential analysis. Therefore, the low number of biexponential pixels in experiment 1 could also represent a consequence of these experimental constraints. In experiment 2, we accounted for these experimental restrictions by increasing the number and interval of echo times to cover longer T_2* relaxation times. Nevertheless, in experiment 2, biexponential T_2* decay behavior was still scarce on a voxel-by-voxel basis. On a small ROI-averaged basis, which incorporates higher SNR values by approximately a factor of 10, the tendon-like region showed preferentially biexponential signal decay for a fiber-to-field angle of 0°, but not for an angle of 55°. At the magic angle (55°), we found a balance between mono- and biexponential decay. We hypothesize here, based on the literature,[12] that the short component of T_2* (bound water) is subject to a stronger orientation dependence than the long component attributable to unaveraged dipolar coupling. This hypothesis could explain, to some extent, the vanishing of the biexponential decay at the magic angle: If it is assumed that the short component (only) exhibits an increase of T_2* toward the long T_2* of the other tissue component approaching the magic angle orientation, then the two components cannot be adequately differentiated anymore by the fitting algorithm. However, our results on ROI-averaged basis indicate that the T_2* decay at magic angle still showed more biexponential decay behavior than at 90°, which is not supported by this hypothesis.

For very large ROIs covering the red zone and white zone of the meniscus, we found a preferential biexponential decay when measured at a fiber-to-field angle of 0°, which indicates that bicomponent analysis could be more relevant for cases where a combination of long and short T_2/T_2* tissues are analyzed together in an ROI (i.e., low-resolution clinical/translational images) and less important when each structure can be resolved using microscopic resolution imaging.

We showed that monoexponential T_2* values varied up to 400% to 500% (for voxel-wise– and ROI–averaged analysis, respectively) with orientation to the magnetic field, especially in the highly anisotropic tendon-like parts of the meniscus. This is in line with the results of Henkelmann et al.,[12] who measured 6 different tissues, including bovine Achilles tendon, and found that particularly short relaxing components of highly organized tissues are affected by relaxation anisotropy attributable to incomplete averaging of dipolar coupling.

Moreover, the results are in accord with the results of Krasnosselskaia et al.,[14] who measured bovine digital flexor tendon and found a factor of 6 change in signal intensity with change in fiber-to-field orientation from the "magic angle" of 54.7° to 0°.

In our study, we found similar orientational fiber-to-field T_2* behavior, as expected on the basis of previous magic-angle studies. Highest T_2* values were found at 55°, the magic angle, where most of the water-related protons precess at comparably similar frequencies. In contrast, lowest values were found at 0°, where the dipolar interaction is at a maximum. Mobile and immobile protons tend to precess at different frequencies, which results in a decrease of effective T_2 and T_2* values. At 90°, the combined effect of the two magic angles, 55° and 125°, does not allow to reach a similar decrease of 0°, and therefore the T_2* values found for this angle are at a level somewhere between the 0° and 55° effect.[17]

In our opinion, this fiber-to-field angle dependence has strong clinical implications not only for quantitative T_2/T_2* mapping, but also for meniscus measurements in general. The reason for that is that T_2* values, T_2 values, and also signal-intensity values of morphological sequences (be it T_2–, T_1–, or PD–weighted images), always (naturally) have some contribution from transversal relaxation time and are affected because of knee positioning in the coil (and thus the fiber-to-field angle). Here, we performed this orientational analysis of the bulk meniscus fibers in terms of T_2* values for the first time, and we showed that for these highly ordered fiber bundles, the angle dependence can be highly significant. Moreover, we believe this should be appropriately taken into consideration in every meniscus MRI measurement to standardize clinical imaging protocols by ensuring similar knee angle and thus fiber-to-field angle and to subsequently avoid misinterpretation.

The findings in this study can also be applied to lower field strength, such as 1.5 and 3 T, where likely a similar bicomponent behavior would be observed. However, lower SNR in lower field strengths will inevitably limit the precision of the bicomponent analysis.

MRI has become the most important tool to assess meniscus health and degeneration and is used for preoperative assessment as well as postoperative follow-up. So far, in clinical routine this assessment is restricted to morphological MRI. However, newly developed quantitative techniques, such as T_2* mapping, might not only improve diagnosis of early degeneration preceding a subsequent tear, but also allow for exact monitoring of disease and repair, which would, in turn, allow for quantitative studies on different surgical treatment options. Both would lead to significant benefits for patients.

There are some limitations in this study. First, within the scope of this MR microscopy study, only a small sample size has been investigated for looking into the main effects of orientation dependence and differentiation between bi- and monoexponential T_2* decay. Consequently, a correlation between T_2* values and a histological score has not been studied. A study including healthy human menisci may address this in future studies; however, healthy ex vivo human meniscus samples were not available for this study. Second, the SNR (~35) and the previously mentioned number of echo

times were relatively low for a thorough biexponential analysis, which potentially affected the outcome of the voxel-wise biexponential analysis. Hence, optimal echo time distribution, number of echo times, and optimal and minimum SNR values for a precise biexponential T_2* mapping of the meniscus should be evaluated in a future biexponential simulation study.

5 | CONCLUSION

In our study, we demonstrated the highest-resolution meniscus measurements to date allowing the identification of meniscus substructures and structural alterations and to quantify T_2*. We found no clear biexponential decay behavior for the meniscal substructures on a small-sized voxel basis. Moreover, a strong orientational dependence of T_2* decay reflecting the anisotropic properties of the meniscal collagen fibers was demonstrated. MR microscopy can help clarify the complexity of the meniscus substructures and might help in the interpretation of moderate resolution T_2/T_2^*-weighted images and T_2* values. The results of this study may support future studies using T_2* mapping techniques to identify patients suffering from early degeneration and monitor therapeutical interventions.

ACKNOWLEDGMENTS

The authors are grateful for the support by the Austrian Science Fund (FWF) KLI 541-B30.

Moreover the financial support by the Austrian Federal Ministry of Science, Research and Economy and the National Foundation for Research, Technology and Development is gratefully acknowledged.

Further acknowledgement goes to Ruth Grübl-Barabas for excellent technical assistance in histological processing.

REFERENCES

1. Kawamura S, Lotito K, Rodeo S. Biomechanics and healing response of the meniscus. *Oper Tech Sports Med*. 2003;11:68-76.
2. Berthiaume MJ, Raynauld JP, Martel-Pelletier J, et al. Meniscal tear and extrusion are strongly associated with progression of symptomatic knee osteoarthritis as assessed by quantitative magnetic resonance imaging. *Ann Rheum Dis*. 2005;64:556-563.
3. Robson MD, Gatehouse PD, Bydder M, Bydder GM. Magnetic resonance: an introduction to ultrashort TE (UTE) imaging. *J Comput Assist Tomogr*. 2003;27:825-846.
4. Tyler DJ, Robson MD, Henkelman RM, Young IR, Bydder GM. Magnetic resonance imaging with ultrashort TE (UTE) PULSE sequences: technical considerations. *J Magn Reson Imaging*. 2007;25(2):279-289.
5. Chu CR, Williams AA, West RV, et al. Quantitative magnetic resonance imaging UTE-T2* mapping of cartilage and meniscus healing after anatomic anterior cruciate ligament reconstruction. *Am J Sports Med*. 2014;42:1847-1856.
6. Williams A, Qian Y, Golla S, Chu CR. UTE-T2 * mapping detects sub-clinical meniscus injury after anterior cruciate ligament tear. *Osteoarthr Cartilage*. 2012;20:486-494.
7. Juras V, Apprich S, Zbyn S, et al. Quantitative MRI analysis of menisci using biexponential T2* fitting with a variable echo time sequence. *Magn Reson Med*. 2014;71:1015-1023.
8. Pauli C, Grogan SP, Patil S, et al. Macroscopic and histopathologic analysis of human knee menisci in aging and osteoarthritis. *Osteoarthr Cartilage*. 2011;19:1132-1141.
9. Herwig J, Egner E, Buddecke E. Chemical changes of human knee joint menisci in various stages of degeneration. *Ann Rheum Dis*. 1984;43:635-640.
10. Diaz E, Chung CB, Bae WC, et al. Ultrashort echo time spectroscopic imaging (UTESI): an efficient method for quantifying bound and free water. *NMR Biomed*. 2012;25:161-168.
11. Fullerton GD, Rahal A. Collagen structure: the molecular source of the tendon magic angle effect. *J Magn Reson Imaging*. 2007;25:345-361.
12. Henkelman RM, Stanisz GJ, Kim JK, Bronskill MJ. Anisotropy of NMR properties of tissues. *Magn Reson Med*. 1994;32:592-601.
13. Peto S, Gillis P. Fiber-to-field angle dependence of proton nuclear magnetic relaxation in collagen. *Magn Reson Imaging*. 1990;8:705-712.
14. Krasnosselskaia LV, Fullerton GD, Dodd SJ, Cameron IL. Water in tendon: orientational analysis of the free induction decay. *Magn Reson Med*. 2005;54:280-288.
15. Xia Y, Moody JB, Alhadlaq H. Orientational dependence of T2 relaxation in articular cartilage: A microscopic MRI (microMRI) study. *Magn Reson Med*. 2002;48:460-469.
16. Szeverenyi NM, Bydder GM. Dipolar anisotropy fiber imaging in a goat knee meniscus. *Magn Reson Med*. 2011;65:463-470.
17. Bydder M, Rahal A, Fullerton GD, Bydder GM. The magic angle effect: a source of artifact, determinant of image contrast, and technique for imaging. *J Magn Reson Imaging*. 2007;25:290-300.
18. Andrews SH, Rattner JB, Abusara Z, Adesida A, Shrive NG, Ronsky JL. Tie-fibre structure and organization in the knee menisci. *J Anat*. 2014;224:531-537.
19. Petersen W, Tillmann B. Collagenous fibril texture of the human knee joint menisci. *Anat Embryol (Berl)*. 1998;197:317-324.
20. Qian Y, Boada FE. Acquisition-weighted stack of spirals for fast high-resolution three-dimensional ultra-short echo time MR imaging. *Magn Reson Med*. 2008;60:135-145.
21. Berg A, Potthast A, Starewicz P MR- Microscopy on a human 7T-scanner. In: Proceedings of the ISMRM/ESMRMB 2010; 2010; Stockholm, Sweden:10482010.
22. Deligianni X, Bar P, Scheffler K, Trattnig S, Bieri O. High-resolution Fourier-encoded sub-millisecond echo time musculoskeletal imaging at 3 Tesla and 7 Tesla. *Magn Reson Med*. 2013;70:1434-1439.
23. Youla DC, Webb H. Image restoration by the method of convex projections: part 1 theory. *IEEE Trans Med Imaging*. 1982;1:81-94.
24. Johnson KM, Fain SB, Schiebler ML, Nagle S. Optimized 3D ultrashort echo time pulmonary MRI. *Magn Reson Med*. 2013;70:1241-1250.

25. Deligianni X, Bar P, Scheffler K, Trattnig S, Bieri O. Water-selective excitation of short T2 species with binomial pulses. *Magn Reson Med*. 2014;72:800-805.
26. Springer F, Steidle G, Martirosian P, et al. Quick water-selective excitation of fast relaxing tissues with 3D UTE sequences. *Magn Reson Med*. 2014;71:534-543.
27. Levenberg K. A method for the solution of certain non-linear problems in least squares. *Quart Appl Math*. 1944;2:164-168.
28. Marquardt D. An algorithm for least-squares estimation of non-linear parameters. *SIAM J Appl Math*. 1963;11:431-441.
29. Markwardt CB. Non-linear least-squares fitting in IDL with MPFIT. *Astronomical Society of the Pacific Conference Series*. 2009;411:251-254.
30. Milford D, Rosbach N, Bendszus M, Heiland S. Mono-exponential fitting in T2-relaxometry: relevance of offset and first echo. *PLoS One*. 2015;10:e0145255.
31. Bevington PR, Robinson K. *Data Reduction and Error Analysis for the Physical Sciences*. 3rd ed. London: McGraw-Hill; 2003.
32. Akaike H. Information theory and an extension of the maximum likelihood principle. In: Petrov BN, Csáki F, eds. *2nd International Symposium on Information Theory, Tsahkadsor, Armenia, USSR, September 2–8, 1971*. Budapest: Akadémiai Kiadó; 1973:267-281.
33. Busca G, Cigado A, Datteo A. Autoregressive Model Applied to the Meazza Stadium for Damage Detection. In: Niezrecki, ed. *Structural Health Monitoring & Damage Detection*. In Proceedings of the 33th IMAC, A Conference and Exposition on Structural Dynamics, 2015. Vol. 7.
34. Hurvich CM, Tsai CL. Regression and time series model selection in small samples. *Biometrika*. 1989;76(2):297-307.
35. Yuan J, Wong OL, Lo GG, Chan HH, Wong TT, Cheung PS. Statistical assessment of bi-exponential diffusion weighted imaging signal characteristics induced by intravoxel incoherent motion in malignant breast tumors. *Quant Imaging Med Surg*. 2016;6:418-429.
36. Bartlett MS. Properties of sufficiency and statistical tests. *Proc Roy Soc Lond Ser A*. 1937;160:268-282.
37. Development Core R. *Team. A language and environment for statistical computing*. Vienna, Austria: R Foundation for Statistical Computing; 2015.
38. Wickham H. *ggplot2: Elegant Graphics for Data Analysis*. New York, NY: Springer-Verlag, New York; 2009.
39. Ahlmann-Eltze C. ggsignif: Significance Brackets for 'ggplot2'. R package version 0.4.0.2017. https://cran.r-project.org/web/packages/ggsignif/. Published August 03, 2017.
40. Zhang Y, Gabr RE, Schar M, Weiss RG, Bottomley PA. Magnetic resonance Spectroscopy with Linear Algebraic Modeling (SLAM) for higher speed and sensitivity. *J Magn Reson*. 2012;218:66-76.
41. Mansfield P, Morris, . *PG. NMR imaging in biomedicine*, vol. ix. New York, NY: Academic; 1982:354 pp.
42. Bae WC, Du J, Bydder GM, Chung CB. Conventional and ultrashort MRI of articular cartilage, meniscus and intervertebral disc. *Top Magn Reson Imaging*. 2010;21(5):275-289.
43. Bernstein MA, King KF. *Zhou XJ. Handbook of MRI Pulse Sequences*, vol. 1017. Amsterdam; Boston, MA: Elsevier Academic; 2004: xxii, 1017 p.
44. Pauli C, Bae WC, Lee M, et al. Ultrashort-echo time MR imaging of the patella with bicomponent analysis: correlation with histopathologic and polarized light microscopic findings. *Radiology*. 2012;264:484-493.

How to cite this article: Hager B, Walzer SM, Deligianni X, et al. Orientation dependence and decay characteristics of T_2* relaxation in the human meniscus studied with 7 Tesla MR microscopy and compared to histology. *Magn Reson Med*. 2019;81:921–933. https://doi.org/10.1002/mrm.27443